pubs.acs.org/Biomac

Article

Modulating the Thermoresponsive Characteristics of PLGA–PEG-PLGA Hydrogels via Manipulation of PLGA Monomer Sequences

SeongHoon Jo, Soonjong Roh, Jaemin Shim, Ji Woong Yu, Youngmee Jung, Woo Young Jang, Bumjoon Seo,* You-Yeon Won,* and Jin Yoo*

Cite This: *Biomacromolecules* 2024, 25, 5374–5386

Read Online

ACCESS | Metrics & More | Article Recommendations | Supporting Information

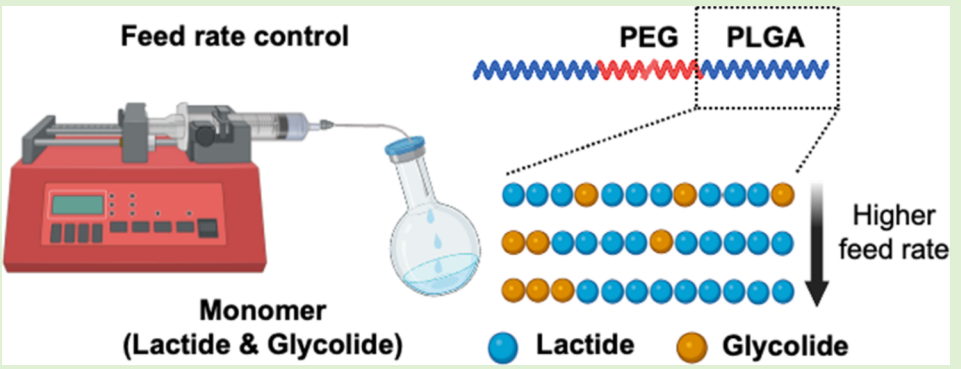

ABSTRACT: Hydrogels are promising materials for biomedical applications, particularly in drug delivery and tissue engineering. This study highlights thermoresponsive hydrogels, specifically poly(lactic-*co*-glycolic acid) (PLGA)–poly(ethylene glycol) (PEG)-PLGA triblock copolymers, and introduces a feed rate-controlled polymerization (FRCP) method. By utilizing an organic catalyst and regulating the monomer feed rate, the sequence distribution of PLGA within the triblock copolymer is controlled. Various analyses, including ^{13}C NMR and rheological measurements, were conducted to investigate the impact of sequence distribution. Results show that altering sequence distribution significantly influences the sol–gel transition, hydrophobicity–hydrophilicity balance, and drug release profile. Increased sequence uniformity lowers the glass transition temperature, raises the sol–gel transition temperature due to enhanced hydrophilicity, and promotes a more uniform drug (curcumin) distribution within the PLGA domain, resulting in a slower release rate. This study emphasizes the importance of PLGA sequence distribution in biomedical applications and the potential of FRCP to tailor thermoresponsive hydrogels for biomedical advancements.

1. INTRODUCTION

Hydrogel plays a pivotal role in biomedical applications, specifically within the realms of wound healing, drug delivery, and tissue engineering. These materials are defined as polymers with a hydrophilic structure, forming a three-dimensional network capable of effectively retaining a substantial amount of water and biological fluids. Noteworthy properties of hydrogel include flexibility, high water absorption capacity in a swollen state, biodegradability, softness, biocompatibility, and tunable mechanical features.[1−3] Among various hydrogels, thermoresponsive hydrogels present compelling advantages in biomedical applications due to their temperature-sensitive behaviors. One of the key advantages of thermoresponsive hydrogels is the ease of application through injectability and conformability to tissue by transitioning into a gel state at body temperature.[4] These hydrogels are commonly associated with physical cross-linking, exhibiting a reversible sol–gel transition in response to temperature changes.[5] Temperature serves as a widely used external stimulus in environment-sensitive systems, particularly relevant for application in tissue engineering and drug delivery.[6−8]

Thermoresponsive hydrogels often have a critical temperature referred to as the lower critical solution temperature (LCST). Below this temperature, the hydrogel exists in a sol (liquid) state, while above it, it undergoes gelation, forming a three-dimensional network. The LCST behavior is typically attributed to temperature-induced changes in hydrophobic–hydrophilic interactions within the polymer chains. Below the LCST, these interactions promote solubility in water, whereas above the LCST, the polymer chains exhibit reduced solubility, leading to gel formation.[9−11] Thermoresponsive hydrogels

Received: June 13, 2024
Revised: July 3, 2024
Accepted: July 3, 2024
Published: July 17, 2024

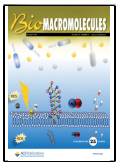

https://doi.org/10.1021/acs.biomac.4c00817
Biomacromolecules 2024, 25, 5374–5386

Scheme 1. Schematic Illustration Depicting the Synthesis of PLGA−PEG-PLGA Triblock Copolymers with Controlled PLGA Sequences Achieved by Manipulating Feed Rates and the Molar Ratio between Lactide (LA) and Glycolide (GL)[a]

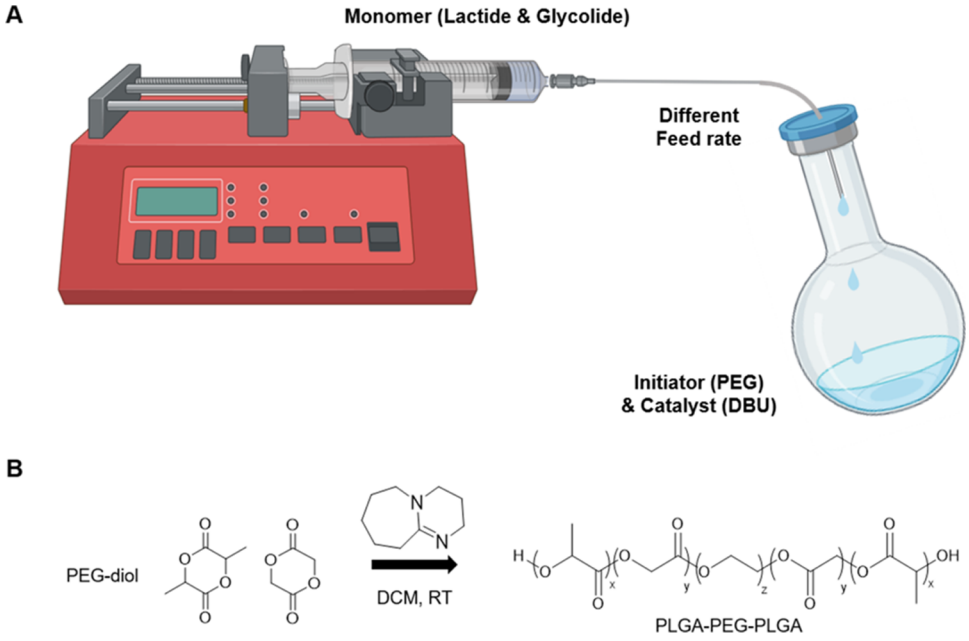

[a](A) Feed rate-controlled polymerization (FRCP). (B) Polymerization of PLGA−PEG-PLGA triblock copolymer using a DBU catalyst. The figure was created with BioRender.com.

have been derived from various polymers, including poly(*N*-isopropylacrylamide) (pNIPAAM),[12,13] poloxamer,[14,15] poly(lactic-*co*-glycolic acid)-poly(ethylene glycol) (PLGA−PEG),[16] and chitosan.[17,18]

In the realm of bioengineering, PLGA−PEG-PLGA triblock copolymers have gained significant traction due to the FDA-approved status of both PEG and PLGA.[19−23] These copolymers find application across diverse biomedical fields,[24,25] including drug release of mechanisms within thermoresponsive hydrogels.[16,26,27] Despite extensive research on factors like lactide (LA) and glycolide (GL) ratio,[28] molecular weight (MW) of PEG and PLGA segments,[29] and total MW,[30] studies specifically investigating the impact of sequence distribution of LA and GL remain scarce.[31]

The limited exploration of sequence distribution effects can be attributed to challenges in controlling the sequence of LA and GL in conventional melt polymerization methods. Typically, the synthesis of PLGA−PEG-PLGA triblock copolymers via melt polymerization has been extensively studied using various metal catalysts such as stannous octoate[32] or zinc alkoxide[19] through ring-opening polymerization (ROP). Efforts to control the randomness of PLGA segment involved employing elevated temperatures (130 or 160 °C) and varying reaction times with the metal catalyst.[31] However, employing a metal catalyst in batch polymerization for sequence control of LA and GL has been found to broaden the MW distribution.[33] In contrast, organic catalysts can facilitate polymerization at room temperature, yielding polymers with narrower MW distributions and avoiding side reactions like transesterification.[34,35]

In our earlier research, we successfully controlled the sequence and randomness of PLGA using semibatch ROP with an organic catalyst, a termed "feed rate-controlled polymerization (FRCP)".[36,37] The impact of sequence distribution on polymer properties, such as PEG crystallization, hygroscopicity, and drug release kinetics, was highlighted in our previous study. Building on these insights, our current research aims to synthesize PLGA−PEG-PLGA triblock copolymers using the FRCP method, as outlined in Scheme 1. LA and GL monomers were used, with PEG-diol as the initiator, and 1,8-diazabicyclo[5,4,0]undec-7-ene (DBU) as the organic catalyst for the ROP reaction.[37,38] Various copolymers with different LA-to-GL ratios were synthesized by continuously injecting a mixture of LA and GL into the PEG-diol initiator at a constant rate while controlling the feed rate. Following synthesis, we assessed the sequence/randomness of these copolymers using ^{13}C NMR and characterized their micelles through dynamic light scattering (DLS), rheological measurements, and drug release profiling.

The results confirmed the ability to modify the sequence distribution in PLGA by controlling the monomer feed rate. Notably, variations in the sequence distribution of PLGA altered its sol−gel transition behavior, thus influencing drug release profile. Therefore, the sequence distribution of PLGA emerges as a critical factor in the formulation of thermosensitive hydrogels, affecting the sol−gel phase transition and the balance between hydrophobicity and hydrophilicity. Furthermore, the synthesized thermoresponsive hydrogel exhibits sprayable properties, underscoring its potential for cutaneous applications. Collectively, this study underscores the importance of controlling the sequence distribution of LA and GL in hydrogel properties, which cannot be achieved through conventional melt/batch copolymerization processes. The FRCP method enables the exploration of sequence distribution effects on hydrogel properties.

2. EXPERIMENTAL SECTION

2.1. Materials. *Rac*-lactide (LA), glycolide (GL), dihydroxy poly(ethylene glycol) (PEG, M_n = 1400 g/mol), benzoic acid, 1,8-diazabicyclo[5.4.0.]undec-7-ene (DBU), dichloromethane (DCM,

https://doi.org/10.1021/acs.biomac.4c00817
Biomacromolecules 2024, 25, 5374−5386

Table 1. Summary of PLGA−PEG-PLGA Triblock Copolymers Synthesized at Various Comonomer Molar Ratios and Feed Rates

copolymer name	LA:GL[b]	feed rate (mL/min)	target molecular weight	actual molecular weight[a]
CP1	2.46:1	0.03	$PL_{1.50k}G_{0.50k}A$-$PEG_{1.4k}$-$PL_{1.50k}G_{0.50k}A$	$PL_{1.46k}G_{0.32k}A$-$PEG_{1.4k}$-$PL_{1.46k}G_{0.32k}A$
CP2	2.46:1	0.05	$PL_{1.50k}G_{0.50k}A$-$PEG_{1.4k}$-$PL_{1.50k}G_{0.50k}A$	$PL_{1.40k}G_{0.28k}A$-$PEG_{1.4k}$-$PL_{1.40k}G_{0.28k}A$
CP3	2.46:1	0.10	$PL_{1.50k}G_{0.50k}A$-$PEG_{1.4k}$-$PL_{1.50k}G_{0.50k}A$	$PL_{1.50k}G_{0.36k}A$-$PEG_{1.4k}$-$PL_{1.50k}G_{0.36k}A$
CP4	5.75:1	0.03	$PL_{1.75k}G_{0.25k}A$-$PEG_{1.4k}$-$PL_{1.75k}G_{0.25k}A$	$PL_{1.45k}G_{0.24k}A$-$PEG_{1.4k}$-$PL_{1.45k}G_{0.24k}A$
CP5	5.75:1	0.05	$PL_{1.75k}G_{0.25k}A$-$PEG_{1.4k}$-$PL_{1.75k}G_{0.25k}A$	$PL_{1.42k}G_{0.15k}A$-$PEG_{1.4k}$-$PL_{1.42k}G_{0.15k}A$
CP6	5.75:1	0.10	$PL_{1.75k}G_{0.25k}A$-$PEG_{1.4k}$-$PL_{1.75k}G_{0.25k}A$	$PL_{1.48k}G_{0.18k}A$-$PEG_{1.4k}$-$PL_{1.48k}G_{0.18k}A$
CP7	9.05:1	0.03	$PL_{1.83k}G_{0.17k}A$-$PEG_{1.4k}$-$PL_{1.83k}G_{0.17k}A$	$PL_{1.70k}G_{0.10k}A$-$PEG_{1.4k}$-$PL_{1.70k}G_{0.10k}A$
CP8	9.05:1	0.05	$PL_{1.83k}G_{0.17k}A$-$PEG_{1.4k}$-$PL_{1.83k}G_{0.17k}A$	$PL_{1.67k}G_{0.11k}A$-$PEG_{1.4k}$-$PL_{1.67k}G_{0.11k}A$
CP9	9.05:1	0.10	$PL_{1.83k}G_{0.17k}A$-$PEG_{1.4k}$-$PL_{1.83k}G_{0.17k}A$	$PL_{1.74k}G_{0.14k}A$-$PEG_{1.4k}$-$PL1.74kG_{0.14k}A$

[a]The LA and GL content of the PLGA segment was determined by ^{1}H NMR. [b]The molar ratio of LA to GL.

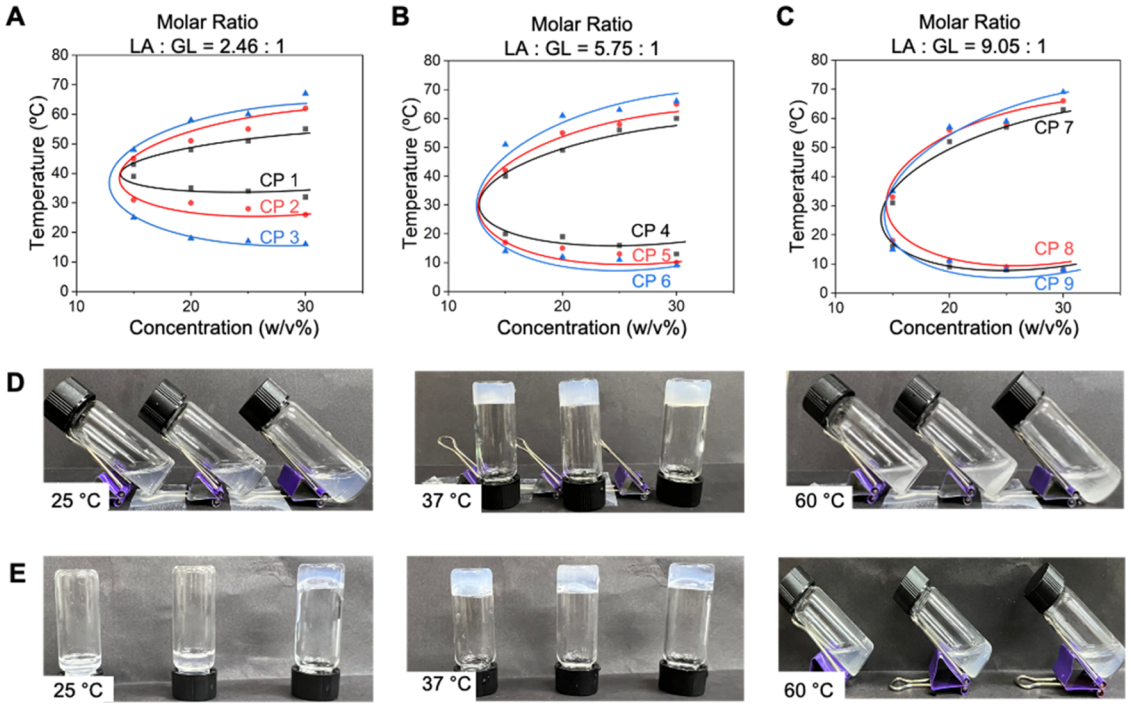

Figure 1. Sol−gel transition curves and phase states of copolymer solutions. (A−C) Sol−gel transition curves for copolymers synthesized at varying feed rates and molar ratios of LA to GL. (D) Images illustrating the sol, gel, and precipitate states of CP1, CP2, and CP3 at different temperatures (25, 37, and 60 °C). The molar ratio and the concentration of the solutions were consistent at LA:GL = 2.46:1 and 15 w/v%. (E) Phase behavior at an increased concentration of 25 w/v%.

99.8%, anhydrous), deuterated chloroform ($CDCl_3$), deuterated dimethyl sulfoxide (DMSO-d_6), 1,1,1,3,3,3-hexafluoro-2-propanol, and curcumin were purchased from Sigma-Aldrich.

2.2. Synthesis of PLGA−PEG-PLGA Triblock Copolymers. PEG−PLGA-PEG triblock copolymers were synthesized using a DBU catalyst, following a previously reported procedure.[36] Briefly, a comonomer solution was prepared by dissolving the appropriate molar ratio of LA and GL in 10 mL of anhydrous DCM. Concurrently, 300 mg of PEG was dissolved in 5 mL of anhydrous DCM within a round-bottom flask, then 30 μL of DBU, dissolved in 1 mL of anhydrous DCM, was added. The comonomer solution was injected using a syringe pump (NE-300 Just Infusion, New Era Pump Systems Inc., NY) at specific feed rates (0.03, 0.05, and 0.10 mL/min), as described in Scheme 1. Additional injections of DBU (30 μL) dissolved in 1 mL of anhydrous DCM were performed when the amount of comonomer solution reached 6.6 and 3.3 mL, respectively (total amount of DBU was 90 μL in 3 mL of anhydrous DCM). Upon completion of comonomer injection, excess benzoic acid (200 mg) was introduced to the reaction mixture to terminate the polymerization. The resulting mixture was slowly poured into 200 mL of isopropanol, followed by centrifugation to collect the PLGA−PEG-PLGA triblock copolymer. The final product was dried under vacuum overnight.

2.3. Characterization of PLGA−PEG-PLGA Triblock Copolymers. ^{1}H and ^{13}C NMR measurements were conducted using a Bruker Avance III 400 MHz NMR spectrometer. For ^{1}H NMR, the samples were dissolved in $CDCl_3$, with chemical shifts referenced to the solvent (7.26 ppm for $CDCl_3$). A coaxial tube was used for ^{13}C NMR measurements, with samples dissolved in 1,1,1,3,3,3-hexafluoro-2-propanol in the outer insert, while DMSO-d_6 served as the solvent for locking and chemical shift reference. The number of measurements was 1024, and the relaxation time was set to 10s. Molecular weights and their distributions were measured using gel permeation chromatography (GPC, Agilent GPC System). $CHCl_3$ was used as the eluent at 40 °C, with a flow rate of 1.0 mL/min. Molecular weights were calibrated against polystyrene (PS) standards. The polymer products listed in Table 1 were calculated based on ^{1}H NMR. PEG analysis was performed using GPC (HLC-8420GPC, Tosoh) with PEG standards and 0.1 M $NaNO_3$ as the eluent from Koptri (Korea Polymer Testing & Research Institute). The result indicated an M_n value of 1400 g/mol.

https://doi.org/10.1021/acs.biomac.4c00817
Biomacromolecules 2024, 25, 5374−5386

2.4. Sol−Gel Phase Transition Curves of Hydrogels. The sol−gel transition of hydrogel was determined using the method described in a previous study.[31] Samples with different concentrations, as shown in Figure 1, were prepared by dissolving the polymer in 1 mL of distilled water and subsequently stored at 4 °C for 24 h. The sol−gel transition and gel−suspension transition were assessed by observing vials, with the temperature incrementing by 1 °C per step from 4 to 70 °C. At each 1 °C temperature increase, the vials were placed in a water bath for 5 min.

2.5. Dynamic Light Scattering (DLS). The measurements of micelle sizes and size distributions at different temperatures were conducted using Zetasizer Nano ZS (Malvern Instruments, U.K.). Hydrodynamic diameters in water were measured at 15, 20, 25, 30, and 37 °C. The samples were measured 3 times at a concentration of 0.5% (w/v). The scattering angle for measurements was set at 90°.

2.6. In Vitro Drug Release Measurements. 30 μg of curcumin was introduced into 1 mL of aqueous polymer solution (20 w/v%) synthesized at various feed rates. The hydrogels were then incubated with 2 mL of PBS at 37 °C and agitated at 120 rpm. 1 mL of PBS was collected at specific time intervals (1, 6 h and 1, 2, 3, 4, 5, 6, 7, 8, 9, 10, 11, 12, 13 days). The cumulative release of curcumin was quantified using a calibration curve, which was obtained by measuring different concentrations of curcumin in PBS after syringe filtration. Absorbance values were measured at 450 nm using a microplate reader (GloMax Discover, Promega). Each experiment was conducted in triplicate.

2.7. In Vitro Degradation of PLGA−PEG-PLGA Hydrogel. PLGA−PEG-PLGA copolymer solutions (20 w/v%, 1 mL each) were prepared in 4 mL vials and incubated in a 37 °C water bath to complete gel formation. Subsequently, 1 mL of PBS (pH 7.4) was added to each vial, and the solutions were shaken at 37 °C and 100 rpm using a shaking incubator (LABTron, Labtron Equipment, U.K.) throughout the degradation period. The PBS in each vial was replaced with the same volume of fresh PBS at specific time intervals (1, 2, 3, 4, 5, 6, 7, 8, 9, 10, 11, 12, 13 days), and the remaining hydrogels were lyophilized using a freeze-dryer (ilShinBioBase, South Korea) and weighed. The copolymer (W_r) was calculated using the equation[39]

$$W_r = W_t - W_s - W_n$$

where W_t is the total weight of the vial with lyophilized hydrogels, W_n is the weight of the vial, and W_s is the salt content in the remaining gels. The salt content was calculated as the difference in weights between the salts initially added to the vial and the sum of salts and the dissolution gel remained in the replaced buffer solutions during the experiment. For GPC measurements, various PLGA−PEG-PLGA copolymer solutions (20 w/v%, 1 mL each) were also prepared in 4 mL vials and incubated in the same shaking incubator at 37 °C with 100 rpm. 1 mL of PBS was added and replaced in each vial at specific time intervals (1, 3, 5, 14 days). A 100 μL sample of the hydrogel was extracted and lyophilized. After freeze-drying for 24 h, each sample was analyzed using GPC (1260 Infinity II, Agilent, CA) with chloroform as the solvent and a flow rate of 1 mL/min.

2.8. Differential Scanning Calorimetry (DSC). Approximately 20 mg of polymers, synthesized at different feed rates, were loaded into sealed aluminum pan. All measurements were performed under a nitrogen purge (50 mL/min). Each sample was placed in the cell of the DSC unit (DSC Q10, TA Instruments, Wilmington, DE). The temperature range was from −60 to 200 °C under a nitrogen atmosphere, with a heating and cooling rate of 10 °C/min.

2.9. Rheology. The sol−gel transition of the copolymer solutions (20 w/v%) was assessed using a rheometer (MCR 102, Anton Paar, Austria) equipped with a parallel plate. For analysis, 370 μL of solution was placed onto a parallel-plate fixture. Measurements of storage modulus (G'), loss modulus (G''), and complex viscosity were conducted. Gelation temperature was determined between 10 and 50 °C with a heating rate of 0.25 °C/min. The angular frequency was fixed at 6.28 rad/s, while maintaining a shear strain of 1%.

2.10. Cell Viability. HDF (Human dermal fibroblast) cells were cultured at 37 °C with 5% CO_2 in Dulbecco's modified Eagle's medium (DMEM) supplemented with 10% (v/v) fetal bovine serum (FBS) and 1% (v/v) penicillin-streptomycin. Cytotoxicity was assessed using the CCK-8 assay kit (Dojindo Laboratories, Kumamoto, Japan). HDF cells were seeded into 12-well plates at a density of 5×10^4 cells/well using Transwell inserts with a pore size of 0.45 μm (Corning, NY). Then, 150 μL of a triblock copolymer solution (20 w/v%) was loaded into the Transwell inserts and placed in individual wells of a 12-well plate, with an insert without the hydrogel serving as the control. HDF cells were exposed to the hydrogels for 24 h, followed by washing twice with Dulbecco's phosphate-buffered saline (DPBS). Afterward, HDF cells were incubated for an additional 4 h at 37 °C with fresh medium and the CCK-8 reagent at a 10:1 ratio, and the absorbance of the supernatant was measured at 450 nm using a microplate reader (GloMax Discover, Promega). Cell viability was assessed by staining the cells using the Live/Dead Viability/Cytotoxicity Assay Kit (Thermo Fisher Scientific, Waltham, MA) and observing them under a fluorescence microscope.

2.11. Dissipative Particle Dynamics (DPD) Simulation. In DPD, the stochastic equation of motion of particle I is described as

$$m_i \dot{\mathbf{v}}_i = \sum_{i \neq j} (F_{ij}^{R} + F_{ij}^{D} + F_{ij}^{R}) = -\frac{\partial V}{\partial \mathbf{r}_i} - \sum_j \gamma \omega^2(r_{ij})(\mathbf{v}_{ij} \cdot \hat{\mathbf{r}}_{ij})\hat{\mathbf{r}}_{ij} + \sum_j \sigma \omega(r_{ij}) \alpha \hat{\mathbf{r}}_{ij} \quad (1)$$

where the three terms on the right-hand side of the equation represent conservative, dissipative, and random forces, respectively.[40,41] Vectors $\mathbf{v}_{ij}$ and $\hat{\mathbf{r}}_{ij}$ denote the relative velocity and the unit displacement vector between atoms i and j. The friction (γ) and noise (σ) parameters are related by the fluctuation−dissipation theorem, $\sigma^2 = 2\gamma k_B T$. α is a Gaussian random number with zero mean and unit variance. Following previous works on the simulation of symmetric CBABC-type block copolymer, we set $\gamma = 4.5$, temperature $T = 1.0$, and weighting function $\omega(r) = 1 - r/r_c$ where $r_c = 1.0$ is the outer cutoff distance. The nonbonded interactions between the beads are described by $V(\mathbf{R}) = \frac{1}{2}\sum_{ij} a_{ij}\omega^2(r_{ij})$, where $\mathbf{R}$ is the set of particle coordinates. For the self-interaction parameters (a_{ii}) and the solvent parameter of hydrophilic PEG chains, the values were set at 25. For the interaction parameters between different types of chains and the solvent parameter of solvophobic PLGA chains, the values were set at $a_{ij} = 35$. Here, two extreme cases where the PLGA sequence is either block or random have been compared for volume fractions in the range of 5−30%. In the random copolymer case, all polymer chains contain monomers with unique random sequences while maintaining the same composition as the block copolymer case. For more details, refer to the Supporting Information.

3. RESULTS AND DISCUSSION

3.1. Synthesis of PLGA−PEG-PLGA Triblock Copolymers. PLGA−PEG-PLGA triblock copolymers were synthesized via the ROP of LA and GL, employing DBU as a catalyst. Achieving control over PLGA sequence and randomness was accomplished through a semibatch ROP method as previously reported.[36] To elucidate, a continuous feed of a mixture of LA and GL was introduced into the PEG-diol initiator at varying feed rates, facilitating control over the PLGA sequence. In this method, the differences in monomer reactivities (GL and LA) become less significant under the condition of a slow comonomer feed limit, wherein the feed rate is slower than the polymerization rates. If the injection rate is sufficiently slow, the rate-determining step of the reaction could shift to the injection step, rather than the bond cleavage step in conventional bath PLGA polymerization methods. This implies that, once the monomers within a droplet are fully consumed and have undergone reaction, the subsequent droplet is introduced into the batch. By employing this

https://doi.org/10.1021/acs.biomac.4c00817
Biomacromolecules 2024, 25, 5374−5386

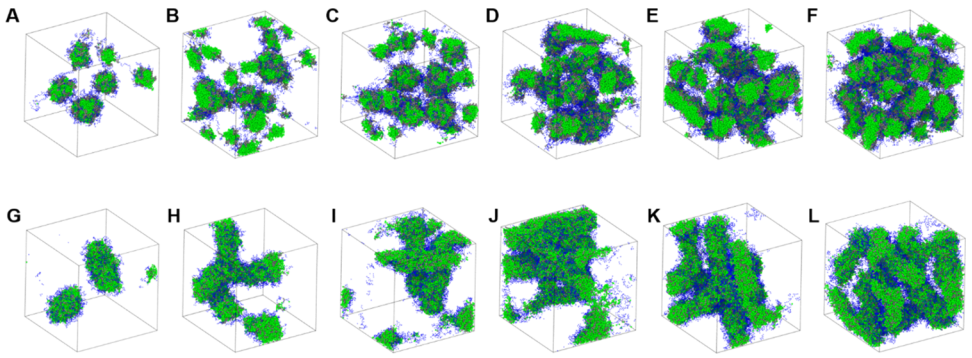

Figure 2. Snapshots of CBABC-type triblock copolymer solutions obtained from DPD simulations. The upper row (A–F) depicts the morphological transition of copolymers with block sequences, while the lower row (G–L) illustrates those of random sequences. The concentrations of the copolymers in the solution are as follows: (A, G) 5 vol%, (B, H) 10 vol%, (C, I) 15 vol%, (D, J) 20 vol%, (E, K) 25 vol%, and (F, L) 30 vol%.

method, we can effectively mitigate the disparate reactivities of monomers, allowing each monomer to be uniformly added to the polymer chain from a global chain standpoint, although locally, some degree of sequence gradient might still not be completely avoidable.

A series of copolymers with varying molar ratios of LA and GL, as well as different monomer feed rates, were designed according to Table 1. The mass ratios of LA and GL were set at 3:1, 7:1, and 11:1, corresponding to the molar ratios of 2.46:1, 5.75:1, and 9.05:1, respectively. Additionally, the reaction was conducted at different feed rates (0.03, 0.05, and 0.10 mL/min) for each molar ratio. The synthesized copolymers (CP1 through CP9) were analyzed using GPC and ^{1}H NMR. Figure S1 illustrates the GPC results, indicating their narrow molecular weight distributions (PDI = 1.13–1.28). This confirms that semibatch polymerization with an organic catalyst offers advantages in achieving a uniform molecular weight distribution compared to conventional tin-catalyzed polymerization reactions. The ^{1}H NMR spectra of CP1–CP9 were utilized to determine their molecular characteristics, specifically their molecular weights based on the molecular weight of the PEG precursor (Figure S2).

3.2. Sol–Gel Transitions of PLGA–PEG-PLGA Copolymers in Aqueous Solution. After mixing CP1–CP9 with DI water, the transition of copolymer solutions with respect to temperature was investigated. The copolymer solutions were placed in an ice–water bath, starting at an initial temperature of 4 °C. Temperature was gradually increased in 1 °C increments to observe the transition of the copolymer solution. The phase transition behavior of the copolymer solution is influenced by factors such as the molecular weights of the PLGA and PEG blocks, overall molecular weight, and variations in copolymer topology.[42] As depicted in Figure 1A–C, the sol–gel transition curves of copolymer solutions exhibited distinct characteristics at different molar ratios of LA and GL. With a given PEG block, the sol–gel transition temperature and critical gel concentration decreased as the LA/GL ratio increased. An increase in the LA molar ratio heightened the polymers' hydrophobicity, as LA is more hydrophobic than GL.[43] Consequently, enhanced hydrophobic interactions led to a more pronounced decrease in the transition temperature in aqueous solution.[28]

Variations in sol–gel curves were observed across different feed rates, reflecting PLGA sequence distributions. Previous study has shown that despite having similar total molecular weights and PEG/PCL ratios, notable differences in sol–gel transition temperatures and gelation windows were evident between PCL–PEG-PCL (1*k*-1*k*-1*k*) and PEG–PCL-PEG (0.55*k*-2*k*-0.55*k*). This underscores the significant impact of copolymer topology on phase transition behavior.[42] Beyond monomer incorporation levels, the polymer's microstructure emerges as a critical determinant of macroscopic behaviors in aqueous solutions. Divergent microstructures arising from varying PLGA sequences, influenced by distinct comonomer feed rates, resulted in distinct behaviors within aqueous solutions.[36]

In contrast to a molar ratio of LA to GL of 2.46:1, when the LA ratio was high and the GL ratio was relatively low, the sol–gel curve showed minimal variation with feed rate. The gelation of PLGA–PEG-PLGA triblock copolymer solutions relied on the hydrophobic PLGA segment. These copolymers formed micelles in water, with the hydrophilic PEG block as the corona and the hydrophobic PLGA segment as the core.[44] Gelation occurred as these micelles transformed; at temperatures below the transition temperature, the copolymers existed in micelle form. As the temperature rose, the hydrophilicity decreased with the collapse of the PEG corona, leading to the formation of a hydrophobic network between neighboring micelles and inducing aggregation.[45] The PLGA sequence effects on the transition temperature of copolymers were maximized at an LA-to-GL molar ratio of 2.46:1. With increasing LA/GL ratio, the hydrophobic LA block became the predominant driver of micelle aggregation, reducing the impact of sequence distribution. Thus, the 2.46:1 molar ratio was selected to characterize PLGA–PEG-PLGA triblock copolymers (CP1, CP2, and CP3) in studies of LA/GL sequence distribution effects.

Figure 1D,E illustrates the phase behaviors of copolymer solutions at 25, 37, and 60 °C. At 15 w/v%, all copolymers (CP1, CP2, and CP3) were in a liquid state at 25 °C, gelled at 37 °C, and precipitated at 60 °C. However, at 25 w/v%, the behavior varied; CP1 and CP2 remained liquid at 25 °C, whereas CP3 gelled. This discrepancy was attributed to variations in the width of the gel window, as observed in the sol–gel transition curve (Figure 1A). This phenomenon indicates an increase in global hydrophobicity from CP1 to CP2 and to CP3.[31]

To characterize the structural and phase behavioral changes associated with the randomness of the PLGA sequence, we conducted DPD simulations comparing the resulting mor-

https://doi.org/10.1021/acs.biomac.4c00817
Biomacromolecules 2024, 25, 5374–5386

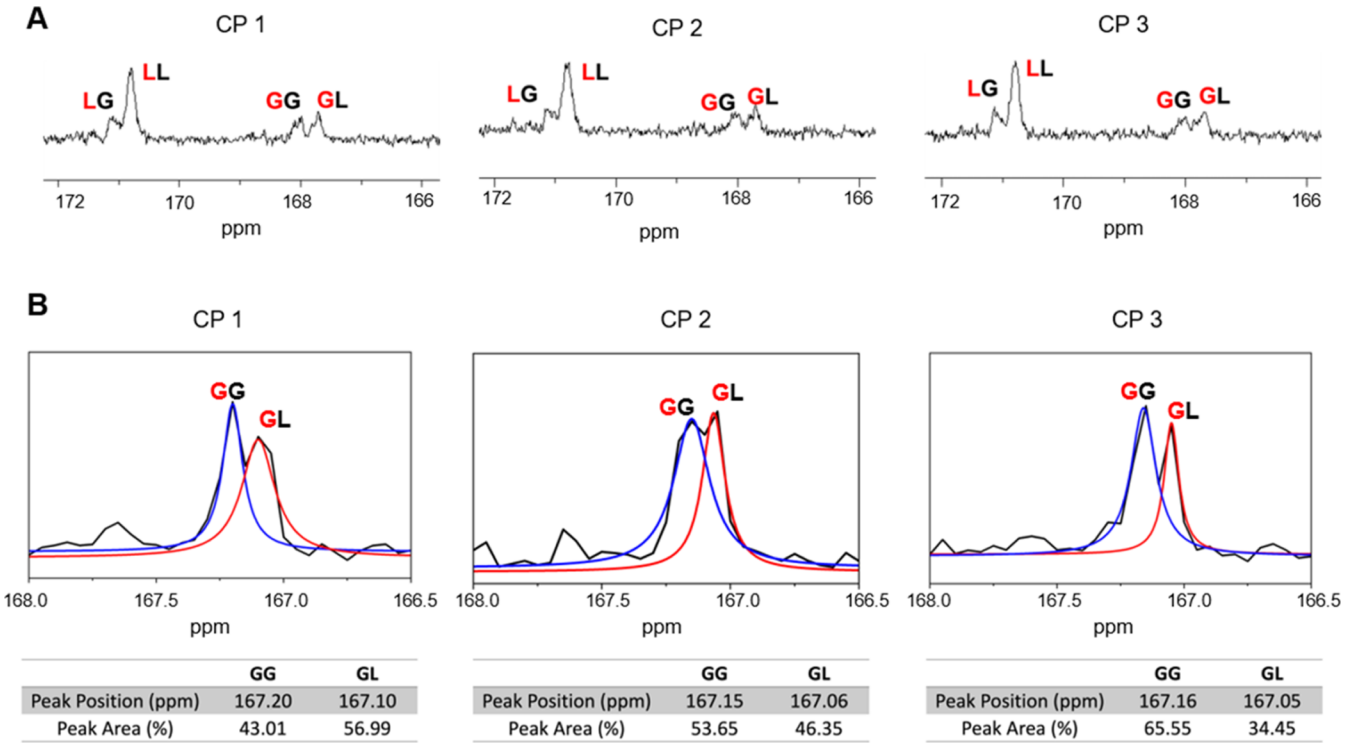

	GG	GL
Peak Position (ppm)	167.20	167.10
Peak Area (%)	43.01	56.99

	GG	GL
Peak Position (ppm)	167.15	167.06
Peak Area (%)	53.65	46.35

	GG	GL
Peak Position (ppm)	167.16	167.05
Peak Area (%)	65.55	34.45

Figure 3. ^{13}C NMR spectra of PLGA−PEG-PLGA triblock copolymers synthesized with different feed rates (CP1, CP2, and CP3). (A) NMR spectra were obtained using a coaxial tube with the polymer/hexafluoroisopropanol solution placed in the outer tube and blank DMSO-d_6 in the inner tube. (B) NMR spectra were obtained using DMSO-d_6 as the solvent. For area analysis, the peaks were assumed to be of Lorentzian shape.

phologies of triblock copolymers with two extreme cases: complete block or complete random PLGA sequences. These two sequences were compared using a fixed set of parameters,[46] by analyzing the resulting morphologies of the triblock copolymer solution across a series of simulations with different concentrations.

At low concentrations, both sequences exhibited the expected formation of a sol phase, characterized by stable micelles suspended in the solution (Figure 2). As the concentration increases, both sequences gradually transitioned to three-dimensional networks formed by the aggregation of micelles, indicating the formation of gel phases. Interestingly, the random sequence demonstrated a sol−gel transition at a higher concentration compared to the block sequence, showcasing a shift from sol to three-dimensional network structures. In contrast, the block sequence displayed a more gradual transition, initially forming of bridges between the micelles. Cluster analysis further supported these observations, revealing a slower decrease in the number of clusters for the random sequence as the concentration increased (Figure S3).

This can be elucidated by examining the micelle structures formed by the two different sequences. In the case of the block sequence, the micelle structure is well defined due to the organization of the hydrophobic PLGA segments. Here, the central core primarily consists of PLA blocks, with PGA blocks attached to its surface, while the PEG blocks reside at the aqueous interface, aiding in the formation of bridges between micelles at concentrations below 5 vol%. On the other hand, the random sequence in copolymers introduces energetically unfavorable close packing in the core. For instance, at 15 vol%, the surface area of the block sequence is nearly twice that of the random sequence. Consequently, micelles in the random sequence merge upon approach without bridges between them. At a higher concentration, around 10 vol%, these enlarged micelles form a network structure extending across the entire simulation box. These findings suggest that the hydrophobicity of the PLGA segments and the interactions between the PLA and PGA blocks contribute to the observed phase behavior differences among copolymers with varying degrees of randomness. Moreover, an increased interaction parameter between the end block and the solvent beads, led to larger domains in copolymers with random sequence compared to the block sequence, indicating earlier precipitation and a narrower window of gelation (Figure S4).

3.3. Characterizations of PLGA−PEG-PLGA Triblock Copolymers. The sequence distribution of LA and GL units in triblock copolymers, CP1, CP2, and CP3, was examined using ^{13}C NMR.[37,47,48] Carbonyl carbon signals were analyzed to determine the cumulative lactate−lactate (LL), lactate-glycolate (LG), glycolate-lactate (GL), and glycolate-glycolate (GG) diad concentrations (I_{LL}, I_{LG}, I_{GL}, and I_{GG}, respectively). Hexafluoroisopropanol was utilized as the solvent for obtaining I_{LL} and I_{LG} data (Figures 3A and S5). Due to the subtle differences in glycolide spectra (i.e., between I_{GL} and I_{GG}) resulting from low glycolide content, the glycolide segments were further analyzed with ^{13}C NMR in DMSO-d_6, fitting the GG (I_{GG}) and GL (I_{GL}) areas with a Lorentzian distribution (Figure 3B). For CP3, the GG peak area was 65.55% and GL was 34.45%. In contrast, CP1 showed a decrease in GG to 43.01% and an increase in GL to 56.99%, indicating a more randomized PLGA sequence with slower comonomer feed rates. An increase in feed rate resulted in longer glycolate sequences, reflecting glycolide's higher reactivity compared to lactide, as supported by the literature.[49,50] The average sequence lengths of lactide ($\bar{L}_L$) and glycolate ($\bar{L}_G$) were determined using eq 2[36]

https://doi.org/10.1021/acs.biomac.4c00817
Biomacromolecules 2024, 25, 5374−5386

Table 2. Cumulative Number-Average Lactate and Glycolate Sequence Lengths for PLGA−PEG-PLGA Triblock Copolymers, Synthesized at Different Feed Rates (with a Lactide-to-Glycolide Molar Ratio of 2.46:1)

copolymer name	feed rate (mL/min)	actual molecular weight	LA:GL	I_{LL}/I_{LG} [a]	$\bar{L}_L$ [a]	I_{GG}/I_{GL} [b]	$\bar{L}_G$ [b]
CP1	0.03	$PL_{1.46k}G_{0.32k}A$-$PEG_{1.4k}$-$PL_{1.46k}G_{0.32k}A$	2.37:1	2.96	7.92	0.99	3.99
CP2	0.05	$PL_{1.40k}G_{0.28k}A$-$PEG_{1.4k}$-$PL_{1.40k}G_{0.28k}A$	2.20:1	3.02	8.03	1.06	4.13
CP3	0.10	$PL_{1.50k}G_{0.36k}A$-$PEG_{1.4k}$-$PL_{1.50k}G_{0.36k}A$	2.48:1	3.16	8.31	1.36	4.72

[a]Determined by ^{13}C NMR spectroscopy in hexafluoroisopropanol as the solvent and calculated using eq 2. [b]Determined by ^{13}C NMR spectroscopy in DMSO-d_6 as the solvent and calculated using eq 2.

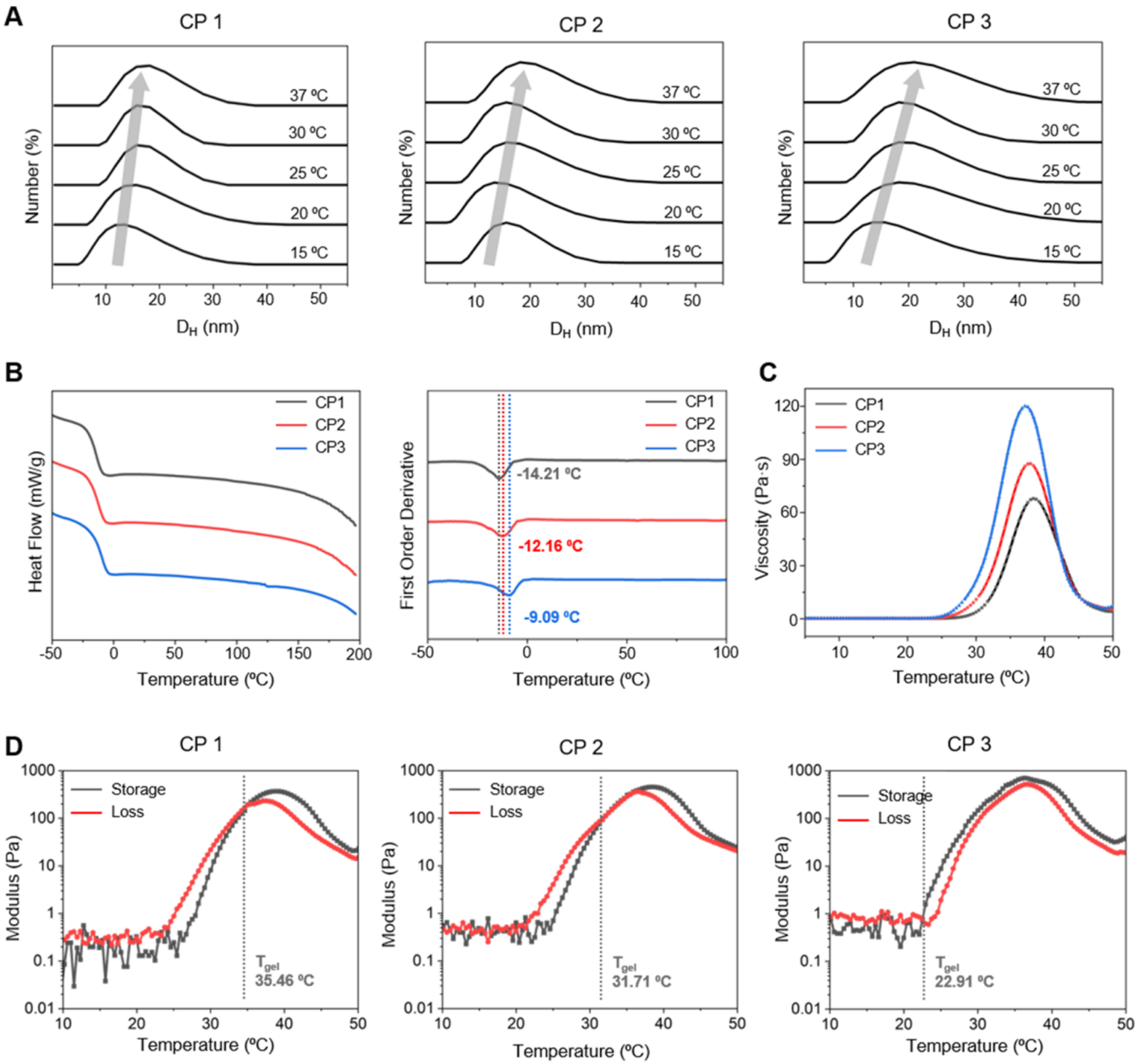

Figure 4. Characterization of the size, thermal, and rheological properties of PLGA−PEG-PLGA triblock copolymer micelles. (A) Distribution of hydrodynamic diameter (D_H) of copolymer micelles determined by DLS at various temperatures, with a copolymer concentration of 0.5 w/v%. (B) Thermograms obtained from DSC showing the T_g's of the triblock copolymers in their neat state. (C, D) Complex viscosity, storage modulus (G'), and loss modulus (G'') of a 20 w/v% aqueous copolymer solution across a temperature range, indicating gelation.

$$\bar{L}_L = 2I_{LL}/I_{LG} + 2;\ \bar{L}_G = 2I_{GG}/I_{GL} + 2 \quad (2)$$

Table 2 illustrates that slower monomer feed rates resulted in shorter lactide and glycolate sequence lengths. For CP1, $\bar{L}_L$ was 7.92 and $\bar{L}_G$ was 3.99, while for CP3, these lengths were 8.31 and 4.72, respectively. This indicates that faster feed rates generate longer glycolate sequences due to the higher reactivity of GL than LA. This trend was also evident in the lactate sequence, where increased feed rates corresponded with larger peak areas, suggesting longer lactate sequences due to the

https://doi.org/10.1021/acs.biomac.4c00817
Biomacromolecules 2024, 25, 5374−5386

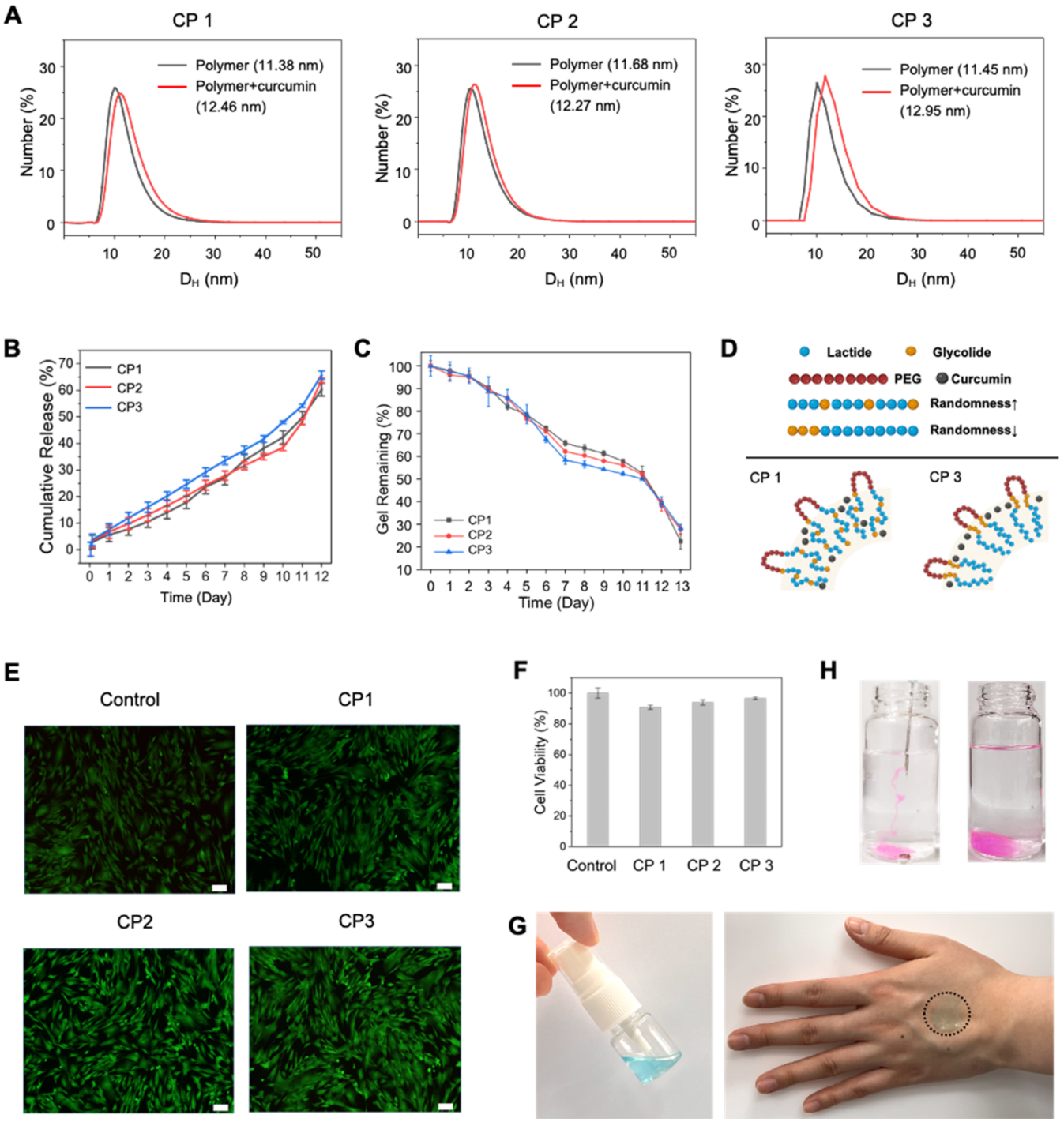

Figure 5. Characteristics of sequenced PLGA hydrogels loaded with curcumin drug. (A) Hydrodynamic diameter distribution of copolymer micelles loaded with curcumin, assessed by DLS. The micelle solution concentration was 0.5 w/v%, at 25 °C. (B) Cumulative release profile of curcumin from PLGA−PEG-PLGA triblock copolymer hydrogel, illustrating the impact of varying monomer sequence distribution characteristics on drug release kinetics. (C) In vitro degradation of the hydrogels monitored over a span of 13 days. (D) Schematic representation of the curcumin release mechanism from the micelle structure. (E) Fluorescence microscopy images showing live/dead HDF cells after exposure to the hydrogels; live cells are stained green, while dead cells are stained red (scale bar = 100 μm). (F) Viability of HDF cells cultured with hydrogels. (G) Demonstration of the sprayable nature of the CP1 hydrogel. (H) Visual demonstration of the rapid gelation of CP1 at 37 °C.

preferential polymerization of GL monomers over LA monomers until GL monomers are depleted.

3.4. Thermal Analysis of PLGA−PEG-PLGA Copolymers. The variations in micelle size and distribution for copolymers, CP1, CP2, and CP3, were analyzed using dynamic light scattering (DLS), as depicted in Figure 4A. The copolymer solutions were prepared at a concentration of 0.5 w/v%, and measurements were conducted at temperatures ranging from 15 to 37 °C. As the temperature increased, the hydrodynamic diameter (D_H) of the micelles also increased. Specifically, the D_H of CP1 (feed rate at 0.03 mL/min) increased from 13.5 nm at 15 °C to 18.2 nm at 37 °C. CP2 and

https://doi.org/10.1021/acs.biomac.4c00817
Biomacromolecules 2024, 25, 5374−5386

CP3 exhibited similar trends, with CP2's D_H increasing from 15.7 to 18.2 nm and CP3's from 13.5 to 21.0 nm at the same temperatures, respectively. The PLGA−PEG-PLGA triblock copolymer micelles tended to aggregate with increasing temperature. Moreover, the size distribution broadened with an increase in feed rate. The micellization behavior of PEG-based triblock copolymers is known to be influenced by the chemical structure of the copolymer chains and the balance between hydrophobicity and hydrophilicity.[51,52] With an increase in temperature, the number of micelles and their propensity to form intermicellar bridges increase due to enhanced hydrophobic interactions.[53] Similarly, the micelles of CP1 to CP3 also exhibited the same trends. CP3, synthesized at a relatively high feed rate, demonstrated a longer lactate sequence and greater hydrophobicity, as evidenced by the higher contact angles observed in Figure S6. The average contact angle for CP1 was 18.8°, for CP2 it was 28.8°, and for CP3 it was 36.17°. Given the hydrophilic nature of PEG, all copolymers had contact angles below 90°; however, CP3's highest value suggests increased hydrophobicity, correlating with DLS data.

Differential scanning calorimetry (DSC) thermograms for the copolymers are presented in Figure 4B. An increase in feed rate correlated with a rise in the glass transition temperature (T_g) of the copolymers, with T_g values for CP1, CP2, and CP3 recorded at −14.21, −12.18, and −9.09 °C, respectively. This trend suggests that higher frequencies of lactate-glycolate diads reduce the T_g of the copolymer because the chemical dissimilarity between the two monomer types. The first derivative of the thermogram more clearly highlighted the T_g differences. Previous studies suggest that T_g values are affected by the PEG/PLGA ratio and increase along with the hydrophobicity of the copolymer.[54] The DLS and contact angle measurements reveal that the randomness of the sequence is associated with hydrophobicity; thus, CP3 had the highest T_g.

The viscosity and rheological properties of the copolymers, CP1, CP2, and CP3, exhibited temperature dependence, as shown in Figure 4C,D. Upon heating, the complex viscosity of the copolymer solutions sharply increased, and the storage modulus (G') surpassed the loss modulus (G'') at the gelation temperature (T_{gel}), indicating hydrogel formation. The T_{gel} for CP1 was 35.46 °C, for CP2 it was 31.71 °C, and for CP3 was 22.91 °C, closely following the sol−gel transition curve. Furthermore, as illustrated in Figure 3C, CP3's viscosity began to rise first and reached the highest magnitude, followed by CP2 and CP1. Typically, a complex viscosity of polymer solutions below 1 Pa·s indicates fluidity.[55] The temperature at which the viscosity exceeds 1 Pa·s was 24.61 °C for CP3, 25.86 °C for CP2, and 28.36 °C for CP1, implying that CP3 gelled first. This phenomenon is attributed to the varying hydrophobicity levels of the PLGA blocks within the copolymers. Decreased randomness (increased blockiness) in the PLGA sequence leads to increased GL content near the junction point between the PLGA and PEG blocks. Therefore, the PLGA blocks of CP3, with GL units being less hydrophobic than LA units, more readily escape from a PLGA core domain and enter another core domain, facilitating the formation of intermicellar PEG bridges, and resulting in earlier gelation. The rheological behavior of the copolymers highlights the distinct properties arising from hydrophobicity, determined by the comonomer sequence distribution of the PLGA.

3.5. Drug Release Properties of Triblock Copolymer Hydrogels. Next, we investigated how the PLGA sequence distribution affects the drug release properties of triblock hydrogels. Curcumin-loaded PLGA−PEG-PLGA micelles were prepared from CP1, CP2, and CP3. The change in D_H upon loading curcumin into the micelles of CP1, CP2, and CP3 was examined using DLS, as shown in Figure 5A. The concentration of the polymer micelle solution was 0.5 w/v%. The sizes of the polymer micelles were 11.38 ± 4.17 nm for CP1, 11.68 ± 4.41 nm for CP2, and 11.45 ± 4.49 nm for CP3. Postcurcumin loading, the observed size were 12.46 ± 4.72, 12.27 ± 4.59, and 12.95 ± 4.66 nm for CP1, CP2, and CP3, respectively, indicating no significant change. These results confirm the stability of the micelles upon drug encapsulation.

Figure 5B illustrates the drug release profile from PLGA−PEG-PLGA copolymer hydrogels, monitored over a 12-day period using curcumin as a model drug. Notably, CP3 exhibited the most rapid release, with 65.72% of curcumin released over 12 days, compared to 60.22% from CP1 within the same duration. The released amount of curcumin was determined by fitting the data to a calibration curve of different curcumin concentrations (Figure S7). Zero-order kinetic models applied over an 11-day period yielded regression coefficients of 0.9846, 0.9886, and 0.9959 for CP1, CP2, and CP3, respectively. Regression coefficients of zero-order kinetics including days 12 and 13 are depicted in Figure S8A, indicating a consistent release of curcumin from the hydrogels over the 12-day period. Hydrogel degradation commenced on day 12 in PBS, as shown in Figure S8B. Previous studies reported curcumin release from PLGA hydrogels or nanoparticles typically occurring over 5−8 days.[56,57] A notable initial burst release of 32.85% curcumin from lipid nanoparticles within the first 2 h, followed by sustained release over 10 days, has been documented.[58] However, the copolymer hydrogels developed in this study sustained the release of curcumin over 12 days.

From day 12 onward, an accelerated release phase was observed, attributed to hydrogel degradation, eventually leading to complete depletion of the drug (Figure S8C).[59] Additionally, the in vitro degradation of the hydrogels was examined by measuring the change in weight over 13 days in PBS at 37 °C. Figure 5C illustrates the percentage of remaining PLGA−PEG-PLGA triblock copolymer hydrogel during degradation. Notably, CP3 exhibited the most rapid degradation between day 5 and day 12 compared to CP1 and CP2. The molecular weights were measured by GPC over time, and the results are displayed in Figure S9. In the GPC analysis, CP3 exhibited the largest shift in GPC traces, and its PDI value peaked on day 14, indicating the fastest in vitro degradation. The degradation and release rates are influenced by the sequence distribution within the PLGA block.[59−62] The order of increasing diad cleavage rate (GG > GL/LG > LL) corresponds to different hydrolytic cleavage rates within the PLGA block.[63] GG linkages cleave more rapidly than GL/LG linkages, which in turn cleave faster than the hydrophobic LL linkages. The cumulative curcumin release appears to correlate with the cleavage rate; CP3, characterized by the highest GG diad content, exhibited the fastest degradation and curcumin release rate.

The variance in drug release kinetics observed among CP1, CP2, and CP3 should also be attributed to the drug's distribution within the PLGA domain. Considering the solubility parameter values of PLA and PGA ($\delta_{PLA} \cong 21.4$ $(J/cc)^{1/2}$, and $\delta_{PGA} \cong 23.8$ $(J/cc)^{1/2}$) and that of curcumin

https://doi.org/10.1021/acs.biomac.4c00817
Biomacromolecules 2024, 25, 5374−5386

($\delta_{curcumin} \approx 25.64$ (J/cc)$^{1/2}$),[43,64] the Flory–Huggins interaction parameters for curcumin with PLA and PGA are estimated to be $\chi_{curcumin/PLA} \cong 1.77$ and $\chi_{curcumin/PGA} \cong 0.33$, respectively, at 25 °C.[65] These values suggest that curcumin is more miscible with PGA than with PLA, leading to a greater association with the GL-rich regions over LA regions in PLGA–PEG-PLGA micelles. In an aqueous environment, the PLGA blocks of the copolymers form hydrophobic core domains (Figure S10). The core domain of a CP3 micelle, characterized by reduced randomness (greater blockiness) and longer glycolate sequences, attracts curcumin to the periphery of the micelle core domain due to its higher affinity for GL. The region near the aqueous-core interface is enriched with GL units, while the LA units predominantly reside deeper within the core. In contrast, the curcumin distribution in CP1 micelles is more homogeneous within the core domain. Consequently, curcumin is released more rapidly from CP3 compared to CP1 and CP2, validating that the monomer sequence length/distribution plays a pivotal role in PLGA modulating curcumin release kinetics in PLGA. This mechanism is schematically depicted in Figure 5D.

Live/dead staining and cell viability assays of HDF cells indicate that hydrogels derived from CP1, CP2, and CP3 exhibit low cytotoxicity, as illustrated in Figure 5E,F. The cell viability for CP1, CP2, and CP3 was measured at 90.9, 94.0, 96.6%, respectively. These findings suggest that the hydrogels of CP1, CP2, and CP3 are biocompatible and hold promise for various biomedical applications. Notably, the very short gelation time of a few seconds establishes the potential for these hydrogels to be utilized as sprayable hydrogels, as depicted in Figure 5G. Initially, the aqueous solution of CP1, at a concentration of 20 w/v%, remained in the liquid phase at room temperature. However, upon application by spraying onto a surface, such as the hand, the solution promptly transitioned to a gel phase. Furthermore, the injectability of these hydrogels was evaluated based on their thermoresponsive rapid gelation properties. Figure 5H presents visual documentation of CP1 during the injection process, demonstrating immediate gelation as the copolymer solution was extruded from a syringe into water at 37 °C.

4. CONCLUSIONS

In this investigation, we have effectively manipulated the sequence distribution of PLGA in PLGA–PEG-PLGA triblock copolymers using the feed rate-controlled polymerization (FRCP) method with DBU as an organic catalyst. Unlike traditional metal catalysts commonly employed for synthesizing such copolymers, DBU facilitates polymerization at ambient temperatures and yields polymers with more uniform molecular weight distributions. We have verified variations in the sequence and degree of randomness of the PLGA block across different feed rates using ^{13}C NMR spectroscopy. The resulting property modifications were analyzed through various techniques, including DLS, rheology, and drug release profiling. These copolymers exhibited varied sol–gel transitions and thermoresponsive behaviors, underscoring the impact of monomer sequence distribution. This effect of the randomness of the PLGA segment on the sol–gel phase behavior was further supported by DPD simulations, which revealed that the increased blockiness of the segment leads to earlier gelation due to enhanced micellar ordering and facilitated bridge formation. The drug release profiles were also found to be directly influenced by the sequence distribution of PLGA, likely due to its impact on the drug's distribution within the PLGA domain. Furthermore, the copolymers exhibited low cytotoxicity, as evidenced by high cell viability (over 90%) in HDF cells. Notably, the thermoresponsive hydrogels formulated from these copolymers demonstrated sprayability, enhancing their potential for biomedical applications. The synthesis of such biocompatible, sprayable hydrogels with tunable drug release profiles represents a significant advancement, rendering them a versatile platform suitable for various fields.

■ ASSOCIATED CONTENT

Supporting Information

The Supporting Information is available free of charge at https://pubs.acs.org/doi/10.1021/acs.biomac.4c00817.

Characterization of PLGA–PEG-PLGA triblock copolymers; GPC, ^{1}H NMR, and ^{13}C NMR spectra; detailed information on DPD simulations; contact angles of the copolymers; in vitro degradation data (PDF)

■ AUTHOR INFORMATION

Corresponding Authors

Bumjoon Seo − *Department of Chemical Biological Engineering, Seoul National University of Science and Technology, Seoul 01811, Republic of Korea;* orcid.org/0000-0002-5029-1593; Email: bseo@seoultech.ac.kr

You-Yeon Won − *Davidson School of Chemical Engineering, Purdue University, West Lafayette, Indiana 47907, United States; Purdue University Center for Cancer Research, Purdue University, West Lafayette, Indiana 47906, United States;* orcid.org/0000-0002-8347-6375; Email: yywon@purdue.edu

Jin Yoo − *Center of Biomaterials, Biomedical Research Institute, Korea Institute of Science and Technology (KIST), Seoul 02792, Republic of Korea; Division of Bio-Medical Science and Technology, KIST School, Korea University of Science and Technology (UST), Seoul 02792, Republic of Korea;* orcid.org/0000-0002-6627-6785; Email: jyoo@kist.re.kr

Authors

SeongHoon Jo − *Center of Biomaterials, Biomedical Research Institute, Korea Institute of Science and Technology (KIST), Seoul 02792, Republic of Korea*

Soonjong Roh − *Center of Biomaterials, Biomedical Research Institute, Korea Institute of Science and Technology (KIST), Seoul 02792, Republic of Korea; Department of Applied Bioengineering, Graduate School of Convergence Science and Technology, Seoul National University, Seoul 08826, Republic of Korea*

Jaemin Shim − *Department of Chemical Biological Engineering, Seoul National University of Science and Technology, Seoul 01811, Republic of Korea*

Ji Woong Yu − *Center for AI and Natural Sciences, Korea Institute for Advanced Study, Seoul 02455, Republic of Korea;* orcid.org/0000-0001-8479-401X

Youngmee Jung − *Center of Biomaterials, Biomedical Research Institute, Korea Institute of Science and Technology (KIST), Seoul 02792, Republic of Korea; Division of Bio-Medical Science and Technology, KIST School, Korea University of Science and Technology (UST), Seoul 02792, Republic of Korea;* orcid.org/0000-0002-4778-4629

https://doi.org/10.1021/acs.biomac.4c00817
Biomacromolecules 2024, 25, 5374−5386

Woo Young Jang − *Department of Orthopedic Surgery, Korea University College of Medicine, Seoul 02841, Republic of Korea; Institute of Nano, Regeneration, Reconstruction, Korea University, Seoul 02841, Republic of Korea*

Complete contact information is available at: https://pubs.acs.org/10.1021/acs.biomac.4c00817

Author Contributions

S.H.J.: Writing—original draft, visualization, validation, methodology, investigation, data curation, conceptualization. S.R.: Methodology, investigation. J.S.: Investigation. J.W.Y.: Investigation. Y.J.: Conceptualization, supervision. W.Y.J.: Funding acquisition, conceptualization. B.S.: Methodology, investigation, writing—review and editing. Y.-Y.W.: Writing—review and editing, supervision, conceptualization. J.Y.: Writing—review and editing, supervision, funding acquisition, conceptualization.

Notes

The authors declare no competing financial interest.

■ ACKNOWLEDGMENTS

This work was financially supported in part by the National R&D Program through the National Research Foundation of Korea (NRF) grant funded by the Ministry of Science and ICT (grant nos. RS-2023-00211412, RS-2023-00302145, 2021M3H4A1A04092879) and KIST research program (2E33151, 2E3312L). Y.-Y.W. acknowledges the support from the US NSF under grant number CBET-1803968. The authors also acknowledge Prof. Yong Joo Kim (Korea University) for helpful discussions. TOC created with Biorender.com.

■ REFERENCES

(1) Caló, E.; Khutoryanskiy, V. V. Biomedical applications of hydrogels: A review of patents and commercial products. *Eur. Polym. J.* **2015**, *65*, 252−267.

(2) Ahmad, S.; Ahmad, M.; Manzoor, K.; Purwar, R.; Ikram, S. A review on latest innovations in natural gums based hydrogels: Preparations & applications. *Int. J. Biol. Macromol.* **2019**, *136*, 870−890.

(3) Volpi, M.; Paradiso, A.; Costantini, M.; Swieszkowski, W. Hydrogel-Based Fiber Biofabrication Techniques for Skeletal Muscle Tissue Engineering. *ACS Biomater. Sci. Eng.* **2022**, *8* (2), 379−405.

(4) Hoffman, A. S. Hydrogels for biomedical applications. *Adv. Drug Delivery Rev.* **2012**, *64*, 18−23.

(5) Tang, G.; Tan, Z.; Zeng, W.; Wang, X.; Shi, C.; Liu, Y.; He, H.; Chen, R.; Ye, X. Recent Advances of Chitosan-Based Injectable Hydrogels for Bone and Dental Tissue Regeneration. *Front. Bioeng. Biotechnol.* **2020**, *8*, No. 587658.

(6) Sun, S.; Sun, S.; Sun, Y.; Wang, P.; Zhang, J.; Du, W.; Wang, S.; Liang, X. Bubble-Manipulated Local Drug Release from a Smart Thermosensitive Cerasome for Dual-Mode Imaging Guided Tumor Chemo-Photothermal Therapy. *Theranostics* **2019**, *9* (26), 8138−8154.

(7) Xu, L.; Zhang, W.; Park, H. B.; Kwak, M.; Oh, J.; Lee, P. C. W.; Jin, J. O. Indocyanine green and poly I:C containing thermo-responsive liposomes used in immune-photothermal therapy prevent cancer growth and metastasis. *J. Immunother. Cancer* **2019**, *7* (1), No. 220.

(8) He, H.; Liu, L.; Zhang, S.; Zheng, M.; Ma, A.; Chen, Z.; Pan, H.; Zhou, H.; Liang, R.; Cai, L. Smart gold nanocages for mild heat-triggered drug release and breaking chemoresistance. *J. Controlled Release* **2020**, *323*, 387−397.

(9) Yu, Y.; Cheng, Y.; Tong, J.; Zhang, L.; Wei, Y.; Tian, M. Recent advances in thermo-sensitive hydrogels for drug delivery. *J. Mater. Chem. B* **2021**, *9* (13), 2979−2992.

(10) Fan, R.; Cheng, Y.; Wang, R.; Zhang, T.; Zhang, H.; Li, J.; Song, S.; Zheng, A. Thermosensitive Hydrogels and Advances in Their Application in Disease Therapy. *Polymers* **2022**, *14* (12), No. 2379.

(11) Liow, S. S.; Dou, Q.; Kai, D.; Karim, A. A.; Zhang, K.; Xu, F.; Loh, X. J. Thermogels: In Situ Gelling Biomaterial. *ACS Biomater. Sci. Eng.* **2016**, *2* (3), 295−316.

(12) Gupta, M. K.; Martin, J. R.; Dollinger, B. R.; Hattaway, M. E.; Duvall, C. L. Thermogelling, ABC Triblock Copolymer Platform for Resorbable Hydrogels with Tunable, Degradation-Mediated Drug Release. *Adv. Funct. Mater.* **2017**, *27* (47), No. 1704107.

(13) Gao, Y.; Chen, J.; Han, X.; Pan, Y.; Wang, P.; Wang, T.; Lu, T. A Universal Strategy for Tough Adhesion of Wet Soft Material. *Adv. Funct. Mater.* **2020**, *30* (36), No. 2003207.

(14) Qin, L.; Ling, G.; Peng, F.; Zhang, F.; Jiang, S.; He, H.; Yang, D.; Zhang, P. Black phosphorus nanosheets and gemcitabine encapsulated thermo-sensitive hydrogel for synergistic photothermal-chemotherapy. *J. Colloid Interface Sci.* **2019**, *556*, 232−238.

(15) Lin, Z.; Mei, D.; Chen, M.; Wang, Y.; Chen, X.; Wang, Z.; He, B.; Zhang, H.; Wang, X.; Dai, W.; et al. A comparative study of thermo-sensitive hydrogels with water-insoluble paclitaxel in molecule, nanocrystal and microcrystal dispersions. *Nanoscale* **2015**, *7* (36), 14838−14847.

(16) Lai, M. C.; Chang, K. C.; Hsu, S. C.; Chou, M. C.; Hung, W. I.; Hsiao, Y. R.; Lee, H. M.; Hsieh, M. F.; Yeh, J. M. In situ gelation of PEG-PLGA-PEG hydrogels containing high loading of hydroxyapatite: in vitro and in vivo characteristics. *Biomed. Mater.* **2014**, *9* (1), No. 015011.

(17) Chenite, A.; Chaput, C.; Wang, D.; Combes, C.; Buschmann, M. D.; Hoemann, C. D.; Leroux, J. C.; Atkinson, B. L.; Binette, F.; Selmani, A. Novel injectable neutral solutions of chitosan form biodegradable gels in situ. *Biomaterials* **2000**, *21* (21), 2155−2161.

(18) Supper, S.; Anton, N.; Seidel, N.; Riemenschnitter, M.; Schoch, C.; Vandamme, T. Rheological study of chitosan/polyol-phosphate systems: influence of the polyol part on the thermo-induced gelation mechanism. *Langmuir* **2013**, *29* (32), 10229−10237.

(19) Barakat, I.; Dubois, P.; Jerome, R.; Teyssie, P. Living Polymerization and Selective End Functionalization of e-Caprolactone Using Zinc Alkoxides as Initiators. *Macromolecules* **1991**, *24*, 6542−6545.

(20) Li, Y.; Yang, H. Y.; Lee, D. S. Advances in biodegradable and injectable hydrogels for biomedical applications. *J. Controlled Release* **2021**, *330*, 151−160.

(21) Cui, S.; Wei, Y.; Bian, Q.; Zhu, Y.; Chen, X.; Zhuang, Y.; Cai, M.; Tang, J.; Yu, L.; Ding, J. Injectable Thermogel Generated by the "Block Blend" Strategy as a Biomaterial for Endoscopic Submucosal Dissection. *ACS Appl. Mater. Interfaces* **2021**, *13* (17), 19778−19792.

(22) Cao, D.; Chen, X.; Cao, F.; Guo, W.; Tang, J.; Cai, C.; Cui, S.; Yang, X.; Yu, L.; Su, Y.; Ding, J. An Intelligent Transdermal Formulation of ALA-Loaded Copolymer Thermogel with Spontaneous Asymmetry by Using Temperature-Induced Sol−Gel Transition and Gel−Sol (Suspension) Transition on Different Sides. *Adv. Funct. Mater.* **2021**, *31* (22), No. 2100349.

(23) Mahar, R.; Chakraborty, A.; Nainwal, N.; Bahuguna, R.; Sajwan, M.; Jakhmola, V. Application of PLGA as a Biodegradable and Biocompatible Polymer for Pulmonary Delivery of Drugs. *AAPS PharmSciTech* **2023**, *24* (1), No. 39.

(24) Zou, F.; Jiang, J.; Lu, F.; Ma, X.; Xia, X.; Wang, L.; Wang, H. Efficacy of intradiscal hepatocyte growth factor injection for the treatment of intervertebral disc degeneration. *Mol. Med. Rep.* **2013**, *8* (1), 118−122.

(25) Ma, H.; He, C.; Cheng, Y.; Li, D.; Gong, Y.; Liu, J.; Tian, H.; Chen, X. PLK1shRNA and doxorubicin co-loaded thermosensitive PLGA-PEG-PLGA hydrogels for osteosarcoma treatment. *Biomaterials* **2014**, *35* (30), 8723−8734.

(26) Zentner, G. M.; Rathi, R.; Shih, C.; McRea, J. C.; Seo, M. H.; Oh, H.; Rhee, B. G.; Mestecky, J.; Moldoveanu, Z.; Morgan, M.; Weitman, S. Biodegradable block copolymers for delivery of proteins and water-insoluble drugs. *J. Controlled Release* **2001**, *72*, 203−215.
(27) He, C.; Kim, S. W.; Lee, D. S. In situ gelling stimuli-sensitive block copolymer hydrogels for drug delivery. *J. Controlled Release* **2008**, *127* (3), 189−207.
(28) Qiao, M.; Chen, D.; Ma, X.; Liu, Y. Injectable biodegradable temperature-responsive PLGA-PEG-PLGA copolymers: synthesis and effect of copolymer composition on the drug release from the copolymer-based hydrogels. *Int. J. Pharm.* **2005**, *294* (1−2), 103−112.
(29) Steinman, N. Y.; Haim-Zada, M.; Goldstein, I. A.; Goldberg, A. H.; Haber, T.; Berlin, J. M.; Domb, A. J. Effect of PLGA block molecular weight on gelling temperature of PLGA-PEG-PLGA thermoresponsive copolymers. *J. Polym. Sci., Part A: Polym. Chem.* **2019**, *57*, 35−39.
(30) Chen, L.; Ci, T.; Li, T.; Yu, L.; Ding, J. Effects of Molecular Weight Distribution of Amphiphilic Block Copolymers on Their Solubility, Micellization, and Temperature-Induced Sol−Gel Transition in Water. *Macromolecules* **2014**, *47* (17), 5895−5903.
(31) Yu, L.; Zhang, Z.; Ding, J. Influence of LA and GA sequence in the PLGA block on the properties of thermogelling PLGA-PEG-PLGA block copolymers. *Biomacromolecules* **2011**, *12* (4), 1290−1297.
(32) Kaihara, S.; Matsumura, S.; Mikos, A. G.; Fisher, J. P. Synthesis of poly(L-lactide) and polyglycolide by ring-opening polymerization. *Nat. Protoc.* **2007**, *2* (11), 2767−2771.
(33) Zhang, X.; Jones, G. O.; Hedrick, J. L.; Waymouth, R. M. Fast and selective ring-opening polymerizations by alkoxides and thioureas. *Nat. Chem.* **2016**, *8* (11), 1047−1053.
(34) Dechy-Cabaret, O.; Martin-Vaca, B.; Bourissou, D. Controlled Ring-Opening Polymerization of Lactide and Glycolide. *Chem. Rev.* **2004**, *104*, 6147−6176.
(35) Patil, S.; Yoo, J.; Won, Y.-Y. Investigation of the Mechanisms and Kinetics of DBU-Catalyzed PLGA Copolymerization via a Full-Scale Population Balance Analysis. *Ind. Eng. Chem. Res.* **2021**, *60* (41), 14685−14700.
(36) Yoo, J.; Viswanath, D.; Won, Y. Y. Strategy for Synthesis of Statistically Sequence-Controlled Uniform PLGA and Effects of Sequence Distribution on Interaction and Drug Release Properties. *ACS Macro Lett.* **2021**, *10* (12), 1510−1516.
(37) Qian, H.; Wohl, A. R.; Crow, J. T.; Macosko, C. W.; Hoye, T. R. A Strategy for Control of "Random" Copolymerization of Lactide and Glycolide: Application to Synthesis of PEG-b-PLGA Block Polymers Having Narrow Dispersity. *Macromolecules* **2011**, *44* (18), 7132−7140.
(38) Patil, S. M.; Won, Y.-Y. Effect of Monomer Sequence Distribution on the Glass Transition Temperature of Poly(d,l-lactic-co-glycolic acid) (PLGA). *Macromolecules* **2024**, *57* (10), 4947−4962.
(39) Wang, Q.; Sun, C.; Xu, B.; Tu, J.; Shen, Y. Synthesis, physicochemical properties and ocular pharmacokinetics of thermosensitive in situ hydrogels for ganciclovir in cytomegalovirus retinitis treatment. *Drug Delivery* **2018**, *25* (1), 59−69.
(40) Groot, R. D.; Madden, T. J. Dynamic simulation of diblock copolymer microphase separation. *J. Chem. Phys.* **1998**, *108* (20), 8713−8724.
(41) Groot, R. D.; Warren, P. B. Dissipative particle dynamics: Bridging the gap between atomistic and mesoscopic simulation. *J. Chem. Phys.* **1997**, *107* (11), 4423−4435.
(42) Gong, C.; Shi, S.; Wu, L.; Gou, M.; Yin, Q.; Guo, Q.; Dong, P.; Zhang, F.; Luo, F.; Zhao, X.; et al. Biodegradable in situ gel-forming controlled drug delivery system based on thermosensitive PCL-PEG-PCL hydrogel. Part 2: sol-gel-sol transition and drug delivery behavior. *Acta Biomater.* **2009**, *5* (9), 3358−3370.
(43) Agrawal, A.; Saran, A. D.; Rath, S. S.; Khanna, A. Constrained nonlinear optimization for solubility parameters of poly(lactic acid) and poly(glycolic acid)—validation and comparison. *Polymer* **2004**, *45* (25), 8603−8612.
(44) Cui, S.; Yu, L.; Ding, J. Semi-bald Micelles and Corresponding Percolated Micelle Networks of Thermogels. *Macromolecules* **2018**, *51* (16), 6405−6420.
(45) Cai, C.; Tang, J.; Zhang, Y.; Rao, W.; Cao, D.; Guo, W.; Yu, L.; Ding, J. Intelligent Paper-Free Sprayable Skin Mask Based on an In Situ Formed Janus Hydrogel of an Environmentally Friendly Polymer. *Adv. Healthcare Mater.* **2022**, *11* (12), No. e2102654.
(46) Kim, T. Y.; Hur, S. M.; Ramirez-Hernandez, A. Effect of Block Sequence on the Solution Self-Assembly of Symmetric ABCBA Pentablock Polymers in a Selective Solvent. *J. Phys. Chem. B* **2023**, *127* (11), 2575−2586.
(47) Sun, J.; Walker, J.; Beck-Broichsitter, M.; Schwendeman, S. P. Characterization of commercial PLGAs by NMR spectroscopy. *Drug Delivery Transl. Res.* **2022**, *12* (3), 720−729.
(48) Grijpma, D. W.; Nijenhuis, A. J.; Pennings, A. J. Synthesis and hydrolytic degradation behaviour of high-molecular-weight L-lactide and glycolide copolymers. *Polymer* **1990**, *31*, 2201−2206.
(49) Dobrzynski, P.; Kasperczyk, J.; Janeczek, H.; Bero, M. Synthesis of Biodegradable Copolymers with the Use of Low Toxic Zirconium Compounds. 1. Copolymerization of Glycolide with L-Lactide Initiated by Zr(Acac)4. *Macromolecules* **2001**, *34*, 5090−5098.
(50) Shen, Y.; Li, D.; Kou, X.; Wang, R.; Liu, F.; Li, Z. Ultrafast ring-opening copolymerization of lactide with glycolide toward random poly(lactic-co-glycolic acid) copolymers by an organophosphazene base and urea binary catalysts. *Polym. Chem.* **2022**, *13* (13), 1861−1868.
(51) Jeong, B.; Bae, Y. H.; Kim, S. W. Thermoreversible Gelation of PEG-PLGA-PEG Triblock Copolymer Aqueous Solutions. *Macromolecules* **1999**, *32*, 7064−7069.
(52) Yang, Y. D.; Yang, Z.; Zhou, Z. K.; Attwood, D.; Booth, C. Association of Triblock Copolymers of Ethylene Oxide and Butylene Oxide in Aqueous Solution. A Study of BnEmBn Copolymers. *Macromolecules* **1996**, *29*, 670−680.
(53) Lee, D. S.; Shim, M. S.; Kim, S. W.; Lee, H.; Park, I.; Chang, T. Novel Thermoreversible Gelation of Biodegradable PLGA-block-PEO-block-PLGA Triblock Copolymers in Aqueous Solution. *Macromol. Rapid Commun.* **2001**, *22* (8), 587−592.
(54) Cespi, M.; Bonacucina, G.; Tiboni, M.; Casettari, L.; Cambriani, A.; Fini, F.; Perinelli, D. R.; Palmieri, G. F. Insights in the rheological properties of PLGA-PEG-PLGA aqueous dispersions: Structural properties and temperature-dependent behaviour. *Polymer* **2021**, *213*, No. 123216.
(55) Yang, Y.; Wang, J.; Zhang, X.; Lu, W.; Zhang, Q. A novel mixed micelle gel with thermo-sensitive property for the local delivery of docetaxel. *J. Controlled Release* **2009**, *135* (2), 175−182.
(56) Chereddy, K. K.; Coco, R.; Memvanga, P. B.; Ucakar, B.; des Rieux, A.; Vandermeulen, G.; Preat, V. Combined effect of PLGA and curcumin on wound healing activity. *J. Controlled Release* **2013**, *171* (2), 208−215.
(57) Hu, B.; Gao, M.; Boakye-Yiadom, K. O.; Ho, W.; Yu, W.; Xu, X.; Zhang, X. Q. An intrinsically bioactive hydrogel with on-demand drug release behaviors for diabetic wound healing. *Bioact. Mater.* **2021**, *6* (12), 4592−4606.
(58) Rahman, M. A.; Ali, A.; Rahamathulla, M.; Salam, S.; Hani, U.; Wahab, S.; Warsi, M. H.; Yusuf, M.; Ali, A.; Mittal, V.; Harwansh, R. K. Fabrication of Sustained Release Curcumin-Loaded Solid Lipid Nanoparticles (Cur-SLNs) as a Potential Drug Delivery System for the Treatment of Lung Cancer: Optimization of Formulation and In Vitro Biological Evaluation. *Polymers* **2023**, *15* (3), No. 542.
(59) Yoo, J.; Won, Y. Y. Phenomenology of the Initial Burst Release of Drugs from PLGA Microparticles. *ACS Biomater. Sci. Eng.* **2020**, *6* (11), 6053−6062.
(60) Lu, Y.; Coates, G. W. Pairing-Enhanced Regioselectivity: Synthesis of Alternating Poly(lactic-co-glycolic acid) from Racemic Methyl-Glycolide. *J. Am. Chem. Soc.* **2023**, *145* (41), 22425−22432.
(61) Washington, M. A.; Swiner, D. J.; Bell, K. R.; Fedorchak, M. V.; Little, S. R.; Meyer, T. Y. The impact of monomer sequence and stereochemistry on the swelling and erosion of biodegradable poly(lactic-co-glycolic acid) matrices. *Biomaterials* **2017**, *117*, 66−76.

https://doi.org/10.1021/acs.biomac.4c00817
Biomacromolecules 2024, 25, 5374−5386

(62) Li, J.; Rothstein, S. N.; Little, S. R.; Edenborn, H. M.; Meyer, T. Y. The effect of monomer order on the hydrolysis of biodegradable poly(lactic-co-glycolic acid) repeating sequence copolymers. *J. Am. Chem. Soc.* **2012**, *134* (39), 16352−16359.
(63) Li, J.; Stayshich, R. M.; Meyer, T. Y. Exploiting sequence to control the hydrolysis behavior of biodegradable PLGA copolymers. *J. Am. Chem. Soc.* **2011**, *133* (18), 6910−6913.
(64) Du, Z.; Zhang, Y.; Xu, H.; Lang, M. Functionalized Pluronic-b-poly(epsilon-caprolactone) based nanocarriers of paclitaxel: solubilization, antiproliferative efficacy and in vivo pharmaceutic kinetics. *J. Mater. Chem. B* **2015**, *3* (18), 3685−3694.
(65) Illy, N.; Corcé, V.; Zimbron, J.; Molinié, V.; Labourel, M.; Tresset, G.; Degrouard, J.; Salmain, M.; Guégan, P. pH-Sensitive Poly(ethylene glycol)/Poly(ethoxyethyl glycidyl ether) Block Copolymers: Synthesis, Characterization, Encapsulation, and Delivery of a Hydrophobic Drug. *Macromol. Chem. Phys.* **2019**, *220* (16), No. 1900210.

https://doi.org/10.1021/acs.biomac.4c00817
Biomacromolecules 2024, 25, 5374−5386